# Electronic Raman response in anisotropic metals

Dietrich Einzel[1] and Dirk Manske[2]
[1]*Walther-Meissner-Institut, Bayerische Akademie der Wissenschaften, D-85748 Garching, Germany*
[2]*Max-Planck-Institut für Festkörperforschung, Heisenbergstrasse 1, D-70569 Stuttgart, Germany*
(Received 1 December 2003; published 18 November 2004)

Using a generalized response theory we derive the electronic Raman response function for metals with anisotropic relaxation rates. The calculations account for the long-range Coulomb interaction and treat the collision operator within a charge conserving relaxation time approximation. We extend earlier treatments to finite wave numbers ($|\mathbf{q}| \ll k_F$) and incorporate inelastic electron-electron scattering besides elastic impurity scattering. Moreover we generalize the Lindhard density response function to the Raman case. Numerical results for the quasiparticle scattering rate and the Raman response function for cuprate superconductors are presented.

DOI: 10.1103/PhysRevB.70.172507 PACS number(s): 74.20.Mn, 74.25.Gz, 72.10.Bg

## I. INTRODUCTION

After the discovery of high-$T_c$ superconductors, something of a stir has been caused by the possibility of investigating these systems by Raman scattering experiments. Through its polarization dependence this spectroscopic method allows for detecting anisotropies in quantities like the superconducting gap and the scattering rates characterizing the transport properties. While the gap anisotropies in high-$T_c$ cuprates, as seen in Raman experiments, are theoretically well understood in terms of $d_{y^2-y^2}$ pairing,[1] the important quasiparticle collision effects are much less studied. Early attempts included constant scattering rates,[2] elastic scattering processes[3,4] or described inelastic scattering processes within the Nearly Antiferromagnetic Fermi Liquid (NAFL) model.[5]

In this paper we investigate the general situation of a normal metal by developing a theory of the electronic Raman effect at finite wave numbers $\mathbf{q} \neq 0$ within the RPA response theory and generalize it to include collision effects. A superposition of elastic and inelastic scattering processes is considered with **k**-dependent relaxation rates and deviations from Matthiessen's rule are studied. Having in mind quasi-2D-systems like high-$T_c$ cuprate superconductors, we present a numerical analysis of the inelastic scattering rates and the Raman response functions employing the FLuctuation EXchange (FLEX) approximation which treats the spin fluctuation-limited transport and Cooper-pairing on the same level.

## II. TRANSPORT THEORY AND GENERALIZED RAMAN RESPONSE: NORMAL STATE

We consider a normal metal in which the electronic states are characterized by a momentum $\hbar\mathbf{k}$, an energy dispersion $\epsilon_{\mathbf{k}} = \xi_{\mathbf{k}} + \mu$ (we set the lattice constant to unity)

$$\epsilon_{\mathbf{k}} = t[-2\cos(k_x) - 2\cos(k_y) + 4B\cos(k_x)\cos(k_y)], \quad (1)$$

with $\mu$ being the Fermi energy, the group velocity $\mathbf{v}_{\mathbf{k}} = (1/\hbar)\nabla_{\mathbf{k}}\epsilon_{\mathbf{k}}$, an inverse effective mass tensor $M_{ij}^{-1}(\mathbf{k}) = \partial^2\epsilon_{\mathbf{k}}/\hbar^2\partial k_i \partial k_j$, and an equilibrium Fermi distribution $n_{\mathbf{k}}$ with derivative $\varphi_{\mathbf{k}} = -\partial n_{\mathbf{k}}/\partial\xi_{\mathbf{k}}$. Next we focus on an external perturbation appropriate for a treatment of the electronic Raman response within the effective mass approximation[6–8]

$$U_{\mathbf{k}}^{\mathrm{ext}} = \underbrace{m\hat{\mathbf{e}}^S \cdot \mathbf{M}^{-1}(\mathbf{k}) \cdot \hat{\mathbf{e}}^I}_{\gamma_{\mathbf{k}}} \cdot \underbrace{\frac{e^2}{mc^2}|\mathbf{A}^I||\mathbf{A}|}_{u_\gamma^{\mathrm{ext}}}. \quad (2)$$

Here, $\hat{\mathbf{e}}^I$ and $\hat{\mathbf{e}}^S$ are the unit vectors of the incident and scattered light, respectively, and **A** denotes the vector potential. Then, the response of the electronic system to this perturbation is described within the the quasiclassical limit of the kinetic equation:

$$\omega\delta n_{\mathbf{k}} - \mathbf{q}\cdot\mathbf{v}_{\mathbf{k}} h_{\mathbf{k}} = i\sum_{\nu=e,i}\delta I_{\mathbf{k}}^{\nu}, \quad (3)$$

where we use the definition

$$h_{\mathbf{k}} = \delta n_{\mathbf{k}} + \varphi_{\mathbf{k}}[U_{\mathbf{k}}^{\mathrm{ext}} + V(\mathbf{q})\delta n_1] \quad (4)$$

and $V(\mathbf{q}) = 4\pi e^2/\mathbf{q}^2$ is the Fourier transform of the long range Coulomb interaction. Physical observables are the generalized response functions

$$\delta n_a = \sum_{\mathbf{p}\sigma} a_{\mathbf{p}}\delta n_{\mathbf{p}}, \quad (5)$$

where $a_{\mathbf{p}}$ is the vertex which describes the coupling of $\delta n_a$ to the external perturbation potential. The collision integrals for elastic ($\nu$=e) and inelastic ($\nu$=i) scattering have the form (conserving relaxation time approximation)

$$\delta I_{\mathbf{k}}^{\nu} = -\Gamma_{\mathbf{k}}^{\nu} h_{\mathbf{k}} + \sum_{\mathbf{p}\sigma} C_{\mathbf{kp}}^{\nu} h_{\mathbf{p}},$$

$$C_{\mathbf{kp}}^{\nu} \approx \varphi_{\mathbf{k}} \sum_b \lambda_b^{\nu} \frac{b_{\mathbf{k}}\Gamma_{\mathbf{k}}^{\nu} b_{\mathbf{p}}\Gamma_{\mathbf{p}}^{\nu}}{\sum_{\mathbf{p}\sigma}\varphi_{\mathbf{p}} b_{\mathbf{p}}^2 \Gamma_{\mathbf{p}}^{\nu}}. \quad (6)$$

The scattering parameters $\lambda_b^{\nu}$ allow a classification of the macroscopic moments $\delta n_b$ [defined through Eq. (5)] into conserved ($\lambda_b^{\nu}$=1) and nonconserved ($\lambda_b^{\nu}$<1) quantities. In what follows we will, for the sake of simplicity, restrict our-

 

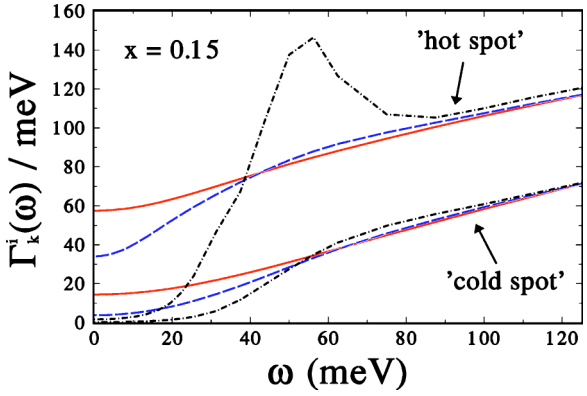


FIG. 1. Calculated inelastic scattering rate $\Gamma^i_{\mathbf{k}}$ versus $\omega$ for the one-band Hubbard model using $U=4t$ at optimal doping ($x=0.15$) for temperatures $T=2T_c$ (solid lines), $T=1.05T_c$ (dashed lines), and $T=0.5T_c$ (dashed–dotted lines).

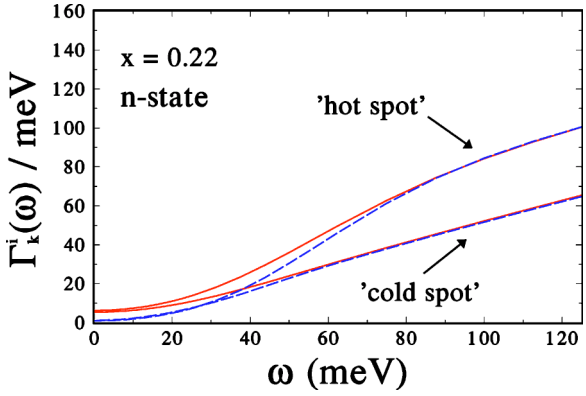


FIG. 2. Inelastic scattering rate $\Gamma^i_{\mathbf{k}}$ versus $\omega$ for the overdoped case ($x=0.22$) using the same notation as in Fig. 1.

selves to the case of charge conservation, i.e., $\lambda^\nu_1=1$, $\lambda^\nu_b=0\ \forall b\neq 1$. While the elastic scattering rate $\Gamma^i_{\mathbf{k}}$ is constant, the inelastic part of the scattering rate $\Gamma^i_{\mathbf{k}}$ has a strong frequency dependence that reflects characteristic lifetime effects, which we discuss below.

In Fig. 1 we show the inelastic scattering rate $\Gamma^i_{\mathbf{k}}(\omega)$ for hole-doped high-$T_c$ cuprates at optimal doping ($x=0.15$) for various temperatures using the FLEX approximation.[9–12] The upper curves correspond to $\mathbf{k}$-directions near $(\pi,0)$ ("hot spots"), the lower ones refer to $\mathbf{k}$ near the diagonal ("cold spots"). For $\omega\to 0$ we find that the inelastic scattering rate at the hot spot is almost three times larger than at the cold spot (solid line). Physically speaking, the scattering rates $\Gamma^i_{\mathbf{k}}$ can be understood in terms of scattering of quasiparticles on spin fluctuations (paramagnons) which are enhanced near the hot spots. In the normal state we also find at small frequencies that the scattering rates decrease with decreasing temperature. For $T<T_c$ a rearrangement of spectral weight occurs reflecting the $\omega$-dependence of the superconducting $d_{x^2-y^2}$-wave gap $\Delta(\omega)$ which is calculated self-consistently.[13] As expected, the maximum is seen at $\omega\simeq 3\Delta_0/\hbar$. In the high-frequency limit, $\Gamma^i_{\mathbf{k}}$ varies linearly with $\omega$ for all $\mathbf{k}$-directions. This is in accordance with both the Marginal (MFL) (Ref. 14) and Nested (NFL) (Ref. 15) Fermi liquid picture.

Let us turn to the overdoped case ($x=0.22$) where we focus on the normal state. Thus, we show in Fig. 2 $\Gamma^i_{\mathbf{k}}$ for the same temperatures and directions as in Fig. 1. Most importantly, the scattering rates become less anisotropic at small frequencies. This is in agreement with Raman scattering experiments where the static scattering rate is extracted for different high-$T_c$ cuprates for different polarizations as a function of the doping concentration.[16,17] Generally speaking, the anisotropy of the scattering rate reflects the anisotropy of the spin fluctuations. Those become less pronounced and more isotropic in the overdoped regime. We still find a reduction of $\Gamma^i_{\mathbf{k}}$ with decreasing temperature and the linear high-frequency behavior remains.

Next, we turn to the generalized theory of Raman scattering. The full response function $\mathcal{L}_{ab}$ for general vertices $a$ and $b$ reads within the RPA [see Eq. (2)]

$$\mathcal{L}_{ab}=\frac{\delta n_a}{\delta u_b^{\mathrm{ext}}}=\underbrace{L_{ab}-\frac{L_{a1}L_{1b}}{L_{11}}}_{\text{TRANSVERSAL}}+\underbrace{\frac{L_{a1}L_{1b}}{L_{11}}\frac{1}{1-IL_{11}}}_{\text{LONGITUDINAL}}. \tag{7}$$

$I$ denotes the corresponding irreducible interaction in a symbolic notation. Note that the decomposition into transverse and longitudinal parts is a general structural property of the respose formalism. For the special case of Raman scattering ($a,b=\gamma_{\mathbf{k}}$) one has to consider the Lindhard response and $(1-IL_{11})$ is the dielectric function $\epsilon$. Then, the full Raman response is of the form

$$L_{\gamma\gamma}(\mathbf{q},\omega)=\frac{\delta n_\gamma(\mathbf{q},\omega)}{u^{\mathrm{ext}}_\gamma(\mathbf{q},\omega)}=M^*_{\gamma\gamma}-\frac{M^{*2}_{\gamma 1}}{M^*_{11}}\left(1-\frac{1}{\epsilon}\right)-\Xi^*_{\gamma\gamma}+\frac{\Xi^{*2}_{\gamma 1}}{\Xi^*_{11}}+\frac{\Xi^*_{11}\zeta^*_{\gamma\gamma}}{\varepsilon}+O\left(\mathbf{q}^2,\frac{1}{\epsilon}\right). \tag{8}$$

Here, $M^*_{ab}$ is the generalization of the Lindhard function due to the inclusion of collision effects:

$$M^*_{ab}=\frac{\mathbf{q}\cdot(\mathbf{T}^{(0)*}_{ab}+\zeta^*_{ab}\mathbf{T}^{(1)*}_{11}-\mathbf{T}^{(1)*}_{ab})\cdot\mathbf{q}}{i\omega-\mathbf{q}\cdot\mathbf{D}^{(1)*}_{11}\cdot\mathbf{q}}. \tag{9}$$

$\mathbf{T}^{(\mu)*}_{ab}$ are generalizations of the electronic conductivity to general vertices $a$, $b$:

$$\mathbf{T}^{(\mu)*}_{ab}=\sum_{\mathbf{p}\sigma}\left(-\frac{\partial n_{\mathbf{p}}}{\partial\xi_{\mathbf{p}}}\right)f_{\mathbf{p}}\frac{a_{\mathbf{p}}\mathbf{v}_{\mathbf{p}}:b_{\mathbf{p}}\mathbf{v}_{\mathbf{p}}}{-i\omega+\Gamma^*_{\mathbf{p}}}\left(\frac{i\Gamma^*_{\mathbf{p}}}{\omega+i\Gamma^*_{\mathbf{p}}}\right)^\mu, \tag{10}$$

$$f_{\mathbf{p}}=\frac{(\omega+i\Gamma^*_{\mathbf{p}})^2}{(\omega+i\Gamma^*_{\mathbf{p}})^2-(\mathbf{q}\cdot\mathbf{v}_{\mathbf{p}})^2},\quad \Gamma^*_{\mathbf{p}}=\Gamma^e_{\mathbf{p}}+\Gamma^i_{\mathbf{p}}.$$

The quantities $\mathbf{D}^{(\mu)*}_{ab}$ are generalized diffusion tensors

$$\mathbf{D}^{(\mu)*}_{ab}=\frac{\mathbf{T}^{(\mu+1)*}_{ab}}{N^*_{ab}},\quad N^*_{ab}=\sum_{\mathbf{p}\sigma}\left(-\frac{\partial n_{\mathbf{p}}}{\partial\xi_{\mathbf{p}}}\right)\frac{i\Gamma^*_{\mathbf{p}}}{\omega+i\Gamma^*_{\mathbf{p}}}a_{\mathbf{p}}b_{\mathbf{p}}.$$

$\Xi^*_{ab}$ are the collision-limited Raman response functions which have a finite $\mathbf{q}\to 0$ limit:

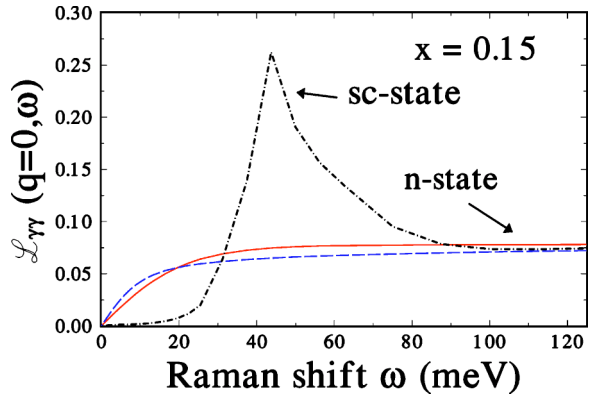


FIG. 3. Full Raman response function $\mathcal{L}_{\gamma\gamma}(\mathbf{q}\to 0,\omega)$ versus $\omega$ at optimal doping ($x=0.15$) for $B_{1g}$ polarization for the same temperatures as in Fig. 1.

$$\Xi^*_{ab}=\sum_{\mathbf{p}\sigma}\left(-\frac{\partial n_{\mathbf{p}}}{\partial\xi_{\mathbf{p}}}\right)f_{\mathbf{p}}\frac{i\Gamma^*_{\mathbf{p}}}{\omega+i\Gamma^*_{\mathbf{p}}}a_{\mathbf{p}}b_{\mathbf{p}} \tag{11}$$

and the objects $\zeta^*_{ab}$ describe the mixing of elastic and inelastic scattering processes and hence deviations from Matthiessen's rule within the conserving relaxation time approximation:

$$\zeta^*_{ab}=\frac{\Xi^*_{a1}\Xi^*_{1b}}{\Xi^{*2}_{11}}+\frac{\omega}{\omega+i\gamma^*}\frac{\Xi^e_{11}\Xi^i_{11}}{\Xi^{*2}_{11}}\times\left(\frac{\Xi^e_{a1}}{\Xi^e_{11}}-\frac{\Xi^i_{a1}}{\Xi^i_{11}}\right)\left(\frac{\Xi^e_{b1}}{\Xi^e_{11}}-\frac{\Xi^i_{b1}}{\Xi^i_{11}}\right)+O(\mathbf{q}^2), \tag{12}$$

$$\gamma^*=\frac{\Xi^*_{11}}{\Xi^e_{11}\Xi^i_{11}}\sum_{\mathbf{p}\sigma}\left(-\frac{\partial n_{\mathbf{p}}}{\partial\xi_{\mathbf{p}}}\right)f_{\mathbf{p}}\frac{i\Gamma^e_{\mathbf{p}}\Gamma^i_{\mathbf{p}}}{\omega+i\Gamma^*_{\mathbf{p}}},$$

$$\Xi^\nu_{ab}=\sum_{\mathbf{p}\sigma}\left(-\frac{\partial n_{\mathbf{p}}}{\partial\xi_{\mathbf{p}}}\right)f_{\mathbf{p}}\frac{i\Gamma^\nu_{\mathbf{p}}}{\omega+i\Gamma^*_{\mathbf{p}}}a_{\mathbf{p}}b_{\mathbf{p}};\quad \nu=e,i.$$

Finally, $\epsilon=\epsilon(\mathbf{q},\omega)=1-V(\mathbf{q})M^*_{11}(\mathbf{q},\omega)$ is the dielectric function of the electronic system mentioned earlier. It has thus been shown that the mixing terms $\propto\zeta^*_{ab}$ in Eq. (8) of the two separate scattering mechanisms occur in the Lindhard function $M^*_{ab}(\mathbf{q},\omega)=O(\mathbf{q}^2)$ and in terms which are screened $\propto\epsilon^{-1}$ by the long range Coulomb interaction. For practical applications of the result shown in Eq. (8) to the cuprate systems, say, where $\mathbf{q}\to 0$ and $\epsilon\approx 10^4$ may be assumed, one may use the $\mathbf{q}\to 0,\epsilon\to\infty$ limit of $L_{\gamma\gamma}$ and the contributions from mixing $\propto\zeta^*_{ab}$ are hence irrelevant. Therefore, the scattering mechanisms can be linearly combined, leading to the exclusive occurrence of $\Gamma^*_{\mathbf{p}}=\Gamma^e_{\mathbf{p}}+\Gamma^i_{\mathbf{p}}$ in the Raman response function. Note that the Raman response function Im $\mathcal{L}_{\gamma\gamma}$ in the limit $\mathbf{q}\to 0$ reduces to Eq. (12) of Ref. 3 where $(\tau^*_L)^{-1}$ corresponds to an average of $\Gamma^*_{\mathbf{p}}$. Hence, this scattering rate can be interpreted as the width of the line shape of Fig. 3 in Ref. 3. Next we focus on the numerical analysis of Im $\mathcal{L}_{\gamma\gamma}$ for a spin-fluctuation based model particularly for the inelastic scattering rate $\Gamma^i_{\mathbf{k}}$.

## III. NUMERICAL CALCULATION OF THE RAMAN RESPONSE

Using normal and anomalous Green's functions, $G$ and $F$, we calculate the full Raman response function via

$$\text{Im}\,\mathcal{L}_{\gamma\gamma}(\mathbf{q}=0,\omega)=\pi\int_{-\infty}^{\infty}d\omega'[f(\omega')-f(\omega'+\omega)]\times\sum_{\mathbf{k}}\tilde{\gamma}(\mathbf{k},\omega',\omega)[N(\mathbf{k},\omega'+\omega)N(\mathbf{k},\omega')-A(\mathbf{k},\omega'+\omega)A(\mathbf{k},\omega')]\gamma(\mathbf{k}), \tag{13}$$

where $N=G''$ and $A=F''$ are the spectral functions (i.e., the **k**-resolved density of states) of the corresponding quasiparticles calculated within the FLEX approximation for the one-band Hubbard model.[9,18] The quantity $\tilde{\gamma}(\mathbf{k},\omega',\omega)$ denotes the renormalized Raman vertex that will be specified below. The bare Raman vertices for the different polarization symmetries considered here, $B_{1g}$, $B_{2g}$, read within the effective mass approximation:

$$\gamma_{B_{1g}}=t[\cos(k_x)-\cos(k_y)],\quad \gamma_{B_{2g}}=4tB\sin(k_x)\sin(k_y).$$

Here, $t$ is the nearest neighbor and $t'=-Bt$ (with $B=0.45$) is the next-nearest neighbor hopping energy of the tight-binding band introduced in Eq. (1). Thus Raman scattering in $B_{1g}$ symmetry mainly probes the "hot regions" while $B_{2g}$ symmetry probes the "cold regions" of the Brillouin zone.

It has been shown earlier that the FLEX approximation yields a phase diagram $T(x)$ for cuprates which is in fair agreement with experiment. One finds a $d_{x^2-y^2}$-wave superconducting order parameter and all characteristic temperature scales.[19] Recently it has also been demonstrated that the resonance peak below $T_c$ in neutron scattering data and angle-resolved photoemission (ARPES) experiments which measure the spectral density entering in Eq. (13) can be well described.[20,13]

While no vertex corrections are considered using the kinetic equation approach, they become important if the FLEX approximation is employed. The main consequence is that the Raman vertex becomes frequency dependent reflecting the retardation effects related to the Cooper-pairing mechanism. In order to calculate the vertex function $\gamma_\nu$ we employ the Nambu notation ($\mu,\nu=0,1,2,3$),[21]

$$P_{\mu\nu}(q)=-\sum_k\frac{1}{2}\text{Tr}[\gamma_\mu G(k+q)\tilde{\gamma}_\nu G(k)] \tag{14}$$

with $q\equiv\mathbf{q},i\nu_m$; $k\equiv\mathbf{k},i\omega_n$; $\Sigma_k=T\Sigma_{i\omega_n}\Sigma_{\mathbf{k}}$, and satisfy the Ward identity $\Sigma_\mu q_\mu\tilde{\gamma}_\mu(k+q,k)=\tau_3G^{-1}(k)-G^{-1}(k+q)\tau_3$. The ladder approximation for the vertex function yields

$$\tilde{\gamma}_\mu(k+q,k)=\gamma_\mu(k+q,k)+\sum_{k'}[\tau_0G(k'+q)\times\tilde{\gamma}_\mu(k'+q,k')G(k')\tau_0P_s(k-k')+\tau_3G(k'+q)\times\tilde{\gamma}_\mu(k'+q,k')G(k')\tau_3P_c(k-k')]. \tag{15}$$

$P_s$ and $P_c$ refer to the spectral function of the spin and charge susceptibility within RPA, respectively, that are defined in

Ref. 9. Finally, the full Raman vertex $\tilde{\gamma}$ satisfies the following integral equation:

$$\tilde{\gamma}(k+Q,k) = \gamma(\mathbf{k}) + \sum_q [P_s(q) + P_c(q)]\tfrac{1}{2}\,\mathrm{Tr}[\tau_3 G(k+q+Q) \times \tau_3 G(k+q)]\tilde{\gamma}(k+q+Q,k+q) \quad (16)$$

and can be derived from Eq. (14) by replacing $\gamma_0$ and $\tilde{\gamma}_0$ by $\gamma\tau_3$ and $\tilde{\gamma}\tau_3$.

## IV. RESULTS FOR $\mathcal{L}_{\gamma\gamma}$ AND DISCUSSION

In Fig. 3 we show our results for the full Raman response function Eq. (8), $\mathcal{L}_{\gamma\gamma}$, for the $B_{1g}$ polarization, which is proportional to the measured Raman intensity, at optimal doping. Both a linear increase and a continuum are found in the limit of low and high frequencies, respectively. This is a direct consequence of the inelastic scattering rate discussed in Fig. 1. In particular, we find an increasing initial slope with decreasing temperature. Below $T_c$ we obtain the usual pair-breaking feature accompanied by a suppression of spectral weight for $\omega \leqslant 2\Delta_0/\hbar$. For low frequencies we also find a power law $\mathcal{L}_{\gamma\gamma} \propto (\omega/2\Delta_0)^3$ that is characteristic for a $d_{x^2-y^2}$-wave gap in the clean limit. Note that the pair breaking peak is finite and renormalized by inelastic quasiparticle scattering processes.

Figure 4 shows the Raman intensity for $B_{2g}$ polarization in the normal state. We again find the high-frequency continuum and an increasing slope of the Raman response function with decreasing temperature. This agrees with the NAFL picture if vertex corrections are considered.[5]

## V. SUMMARY

In summary, we have reconsidered the electronic Raman response with special emphasis on the role of quasiparticle scattering processes. In the normal state a superposition of elastic and inelastic scattering events described by

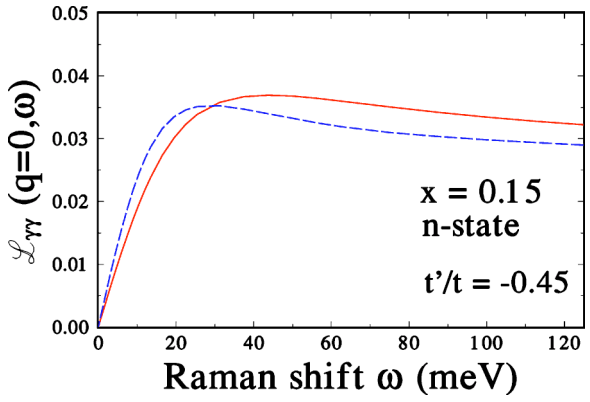


FIG. 4. Full Raman response function $\mathcal{L}_{\gamma\gamma}(\mathbf{q}\to 0,\omega)$ versus $\omega$ at optimal doping ($x=0.15$) for $B_{2g}$ polarization for the same temperatures as in Fig. 1.

**k**-dependent scattering rates leads to a deviation from Matthiessen's rule for the corresponding Raman response functions. These deviations, however, are found to be eliminated by the presence of the long-range Coulomb interaction. We have furthermore studied in detail, the anisotropy of the inelastic scattering rate $\Gamma^i_{\mathbf{k}}$ at optimal doping, and its decrease at higher doping levels towards the overdoped case. The resultant electronic Raman response functions that include the effects of inelastic scattering involving spin fluctuations reproduce the behavior of the normal state characteristic of the phenomenological MFL picture that has been studied in earlier publications.[22] In the superconducting state the inelastic scattering rate becomes gapped due to a frequency dependent $d_{x^2-y^2}$-wave gap, calculated self-consistently, yielding the characteristic shape of the Raman response.[1]

## ACKNOWLEDGMENTS

D.M. thanks the Walther-Meissner-Institute for hospitality and INTAS (Project No. 01-0654) for financial support.

[1] T. P. Devereaux and D. Einzel, Phys. Rev. B **51**, 16 336 (1995); Phys. Rev. B **54**, 15 547 (1996).
[2] L. A. Falkovsky and S. Klama, Physica C **172**, 242 (1990).
[3] A. Zawadowski and M. Cardona, Phys. Rev. B **42**, 10 732 (1990).
[4] D. Einzel and C. Schuster, Czech. J. Phys. **46**, 993 (1996).
[5] T. P. Devereaux and A. P. Kampf, Phys. Rev. B **61**, 1490 (2000); **59**, 6411 (1999).
[6] P. A. Wolff, Phys. Rev. **171**, 436 (1968).
[7] M. C. Krantz and M. Cardona, J. Low Temp. Phys. **99**, 205 (1995); T. Strohm and M. Cardona, Phys. Rev. B **55**, 12 725 (1997).
[8] D. Manske *et al.*, Phys. Rev. B **56**, R2940 (1997).
[9] See, for example, D. Manske *et al.*, Phys. Rev. B **67**, 134520 (2003).
[10] N. E. Bickers *et al.*, Phys. Rev. Lett. **62**, 961 (1989); N. E. Bickers and D. J. Scalapino, Ann. Phys. (N.Y.) **193**, 206 (1989).
[11] T. Dahm and L. Tewordt, Phys. Rev. Lett. **74**, 793 (1995).
[12] M. Langer *et al.*, Phys. Rev. Lett. **75**, 4508 (1995).
[13] D. Manske *et al.*, Phys. Rev. Lett. **87**, 177005 (2001).
[14] C. M. Varma *et al.*, Phys. Rev. Lett. **63**, 1996 (1989).
[15] J. Ruvalds *et al.*, Phys. Rev. B **51**, 3797 (1995).
[16] For a systematic study, see M. Opel *et al.*, Phys. Rev. B **61**, 9752 (2000).
[17] F. Venturini *et al.*, Phys. Rev. Lett. **89**, 107003 (2002).
[18] Note that the NAFL approach of Ref. 5 is restricted to the normal state and thus no spectral function $A$ occurs.
[19] D. Manske *et al.*, Phys. Rev. B **62**, 13 922 (2000); D. Manske *et al.*, *ibid.* **64**, 144520 (2001).
[20] D. Manske *et al.*, Phys. Rev. B **63**, 054517 (2001).
[21] Y. Nambu, Phys. Rev. **117**, 648 (1960).
[22] T. Staufer *et al.*, Solid State Commun. **75**, 975 (1990).